Inorganic Chemistry

Article

pubs.acs.org/IC

Synthesis, Spectral Characterization, Structures, and Oxidation State Distributions in [(corrolato)Fe^{III}(NO)]^n (n = 0, +1, −1) Complexes

Woormileela Sinha,[†] Naina Deibel,[‡,§] Hemlata Agarwala,[#] Antara Garai,[†] David Schweinfurth,[‡] Chandra Shekhar Purohit,[†] Goutam Kumar Lahiri,*[,#] Biprajit Sarkar,*[,‡] and Sanjib Kar*[,†]

[†]School of Chemical Sciences, National Institute of Science Education and Research (NISER), Bhubaneswar, 751005, India

[‡]Institut für Chemie und Biochemie, Anorganische Chemie, Freie Universität Berlin, Fabeckstraße 34-36, D-14195, Berlin, Germany

[§]Institut für Anorganische Chemie, Universität Stuttgart, Pfaffenwaldring 55, D-70550, Stuttgart, Germany

[#]Department of Chemistry, Indian Institute of Technology−Bombay, Powai, Mumbai 400076, India

Supporting Information

ABSTRACT: Two novel *trans*-A_2B-corroles and three [(corrolato){FeNO}^{6}] complexes have been prepared and characterized by various spectroscopic techniques. In the native state, all these [(corrolato){FeNO}^{6}] species are diamagnetic and display "normal" chemical shifts in the ^{1}H NMR spectra. For two of the structurally characterized [(corrolato){FeNO}^{6}] derivatives, the Fe−N−O bond angles are 175.0(4)° and 171.70(3)° (DFT: 179.94°), respectively, and are designated as linear nitrosyls. The Fe−N (NO) bond distances are 1.656(4) Å and 1.650(3) Å (DFT: 1.597 Å), which point toward a significant Fe^{III} → NO back bonding. The NO bond lengths are 1.159(5) Å and 1.162(3) Å (DFT: 1.162 Å) and depict their elongated character. These structural data are typical for low-spin Fe(III). Electrochemical measurements show the presence of a one-electron oxidation and a one-electron reduction process for all the complexes. The one-electron oxidized species of a representative [(corrolato){FeNO}^{6}] complex exhibits ligand to ligand charge transfer (LLCT) transitions (cor(π) → cor(π^*)) at 399 and 637 nm, and the one-electron reduced species shows metal to ligand charge transfer (MLCT) transition (Fe(dπ) → cor(π^*)) in the UV region at 330 nm. The shift of the ν_{NO} stretching frequency of a representative [(corrolato){FeNO}^{6}] complex on one-electron oxidation occurs from 1782 cm^{-1} to 1820 cm^{-1}, which corresponds to 38 cm^{-1}, and on one-electron reduction occurs from 1782 cm^{-1} to 1605 cm^{-1}, which corresponds to 177 cm^{-1}. The X-band electron paramagnetic resonance (EPR) spectrum of one-electron oxidation at 295 K in CH_2Cl_2/0.1 M Bu_4NPF_6 displays an isotropic signal centered at g = 2.005 with a peak-to-peak separation of about 15 G. The in situ generated one-electron reduced species in CH_2Cl_2/0.1 M Bu_4NPF_6 at 295 K shows an isotropic signal centered at g = 2.029. The 99% contribution of corrole to the HOMO of native species indicates that oxidation occurs from the corrole moiety. The results of the electrochemical and spectroelectrochemical measurements and density functional theory calculations clearly display a preference of the {FeNO}^{6} unit to get reduced during the reduction step and the corrolato unit to get oxidized during the anodic process. Comparisons are presented with the structural, electrochemical, and spectroelectrochemical data of related compounds reported in the literature, with a particular focus on the interpretation of the EPR spectrum of the one-electron oxidized form.

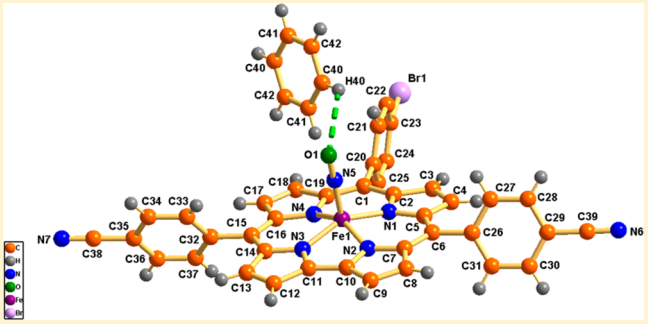

INTRODUCTION

The free radical NO$^\bullet$ acts as a messenger molecule in biological systems by activating the ferrous heme of the guanylate cyclase (sGC).[1] Implications of this signaling behavior have been widely studied by many researchers in chemistry, biology, and medicine. NO$^\bullet$, widely known as reactive nitrogen species (RNS), is also essential for homeostasis of cellular organism.[2] Understanding the mechanism of redox signaling is of great importance from the perspective of physiological functions. Inside cellular organisms, NO$^\bullet$ targets a variety of metalloproteins including hemoglobin and cytochrome c oxidase (CcOx). However, the binding of NO$^\bullet$ with metalloproteins is case sensitive. The binding can be either reversible or irreversible. Methemoglobin, where iron is in the +3 oxidation state, binds NO$^\bullet$ in a reversible fashion, whereas oxyhemoglobin with iron in the +2 oxidation state, binds NO$^\bullet$ in an irreversible fashion.[3] The signaling mechanism of NO$^\bullet$ is directly dependent on the reversible binding of NO$^\bullet$. Thus, it is evident that the mechanism of binding of NO$^\bullet$ with hemoproteins is of considerable importance from a biological and chemical point of view. This has led to the development of an intense research interest in elucidating the mechanism of the interaction of NO$^\bullet$ with hemoproteins and their model

Received: September 11, 2013
Published: January 16, 2014

   dx.doi.org/10.1021/ic402304e | Inorg. Chem. 2014, 53, 1417−1429

Scheme 1. Structures of the A_3-Corrole, 1A, and *trans*-A_2B-Corrole, 2A, and 3A and the Corresponding (A_3-cor) Fe^{III} NO, 1B, and (*trans*-A_2B-cor) $Fe^{III}NO$, 2B and 3B

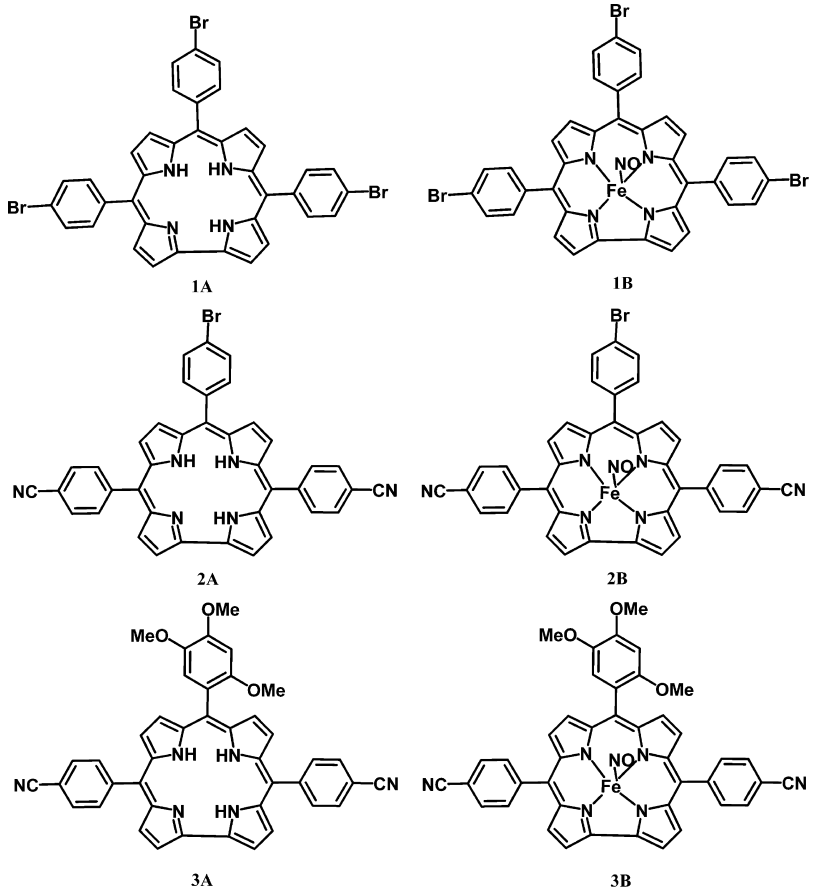

compounds.[3] It is also known that certain enzymes use (macrocycle)FeNO complexes in the oxidized state as transient intermediates for the conversion of nitrite to ammonia.[4] All these observations necessarily point toward the extreme importance of understanding the oxidation state distribution in higher oxidation states of (macrocycle)FeNO systems. Corrole, being a special one among the macrocyclic systems, may be a perfect choice to study the same. In this regard, it should be kept in mind that the corrole ring is just one *meso*-carbon shorter than related porphyrin macrocycle.[5] Compared to porphyrin which has two imino hydrogens, corrole contains three imino hydrogens. Therefore, it can act as a trianionic ligand. Because of the smaller cavity size and more anionic nature of corrole, it tends to stabilize metals in higher oxidation states.[5] In the majority of the cases, in the native state, the oxidation state of metal is one unit higher in metallo-corrole than its metallo-porphyrin analogue. Thus, it has been proven to be easier and more realistic to study the higher oxidation states of metal in corrole based macrocycle.[5] It was also found that in various catalytic reactions, like carbene-tranfer and nitrene-transfer reactions, iron-corrole has been proven to be more superior than its iron-porphyrin analogue.[6] Owing to very limited availability of information, [(corrolato){FeNO}^{6}] complexes[7] could be a perfect choice to study the oxidation state distribution and to get deeper insight into the peculiar reactivities of iron-corrole complexes. A detailed literature survey reveals that there are very few reports on the in situ generated oxidized and reduced species of [(cor){FeNO}^{6}] moieties.[7a,b] cor stands for corrolato and the {FeNO}^{6} nomenclature is based on the Enemark and Feltham notation,[8] where the exponent term six is obtained by using the summation of five iron d-electrons and one unpaired electron from NO. The present work describes the synthesis of one A_3-corrole and two novel *trans*-A_2B-corroles, 5,10,15-tris(4-bromophenyl)corrole, **1A**, 10-(4-bromophenyl)-5,15-bis(4-cyanophenyl)corrole, **2A**, and 10-(2,4,5-trimethoxyphenyl)-5,15-bis(4-cyanophenyl)corrole, **3A** (Scheme 1), and the corresponding one [(A_3-cor){FeNO}^{6}] and two novel [(*trans*-A_2B-cor){FeNO}^{6}] derivatives, namely, [{5,10,15-tris-(4-bromophenyl)cor}{FeNO}^{6}], **1B**, [{10-(4-bromophenyl)-5,15-bis(4-cyanophenyl)cor}{FeNO}^{6}], **2B**, and [{10-(2,4,5-trimethoxyphenyl)-5,15-bis(4-cyanophenyl)cor}{FeNO}^{6}], **3B**. Compared to A_3-corroles, *trans*-A_2B corroles would be more versatile scaffolds and would be a better modulator of the steric and electronic factors for synthesizing a diverse range of metal complexes. A series of electron-withdrawing (like -CN) and -releasing (like -OMe) groups were chosen as substituents in the corrole frameworks keeping in view that these modifications might influence the energies of the molecular orbitals of the respective complexes, thus affecting the spectral features. Moreover, cyanide has been adopted as a substituent in these corroles because of its tendency to get readily converted into a series of other organic functional groups. Thus, these complexes can be considered as potential building blocks for construction of various other metallocorrole-based architectures. Although the syntheses of free base A_3-corrole, **1A**, and [(A_3-cor){FeNO}^{6}], **1B**, have been already reported in the literature,[7d] the crystal structure and UV−vis, IR, and electron

dx.doi.org/10.1021/ic402304e | *Inorg. Chem.* 2014, 53, 1417−1429

paramagnetic resonance (EPR) spectroelectrochemical investigations of **1B** have not been reported so far. The present investigation further relates to the synthesis of two new *trans*-A_2B-corroles, **2A** and **3A** and their corresponding [(cor)-{FeNO}^{6}] derivatives. In addition to the synthesis and spectral characterization of **1A**, **1B**, **2A**, **2B**, **3A**, and **3B**, the crystal structures of **1B** and **2B** and electrochemistry, UV−vis, IR, and EPR-spectroelectrochemical investigations of **1B**, **2B**, and **3B** are also reported here. To garner further support of the experimentally obtained results, we have also carried out density functional theory (DFT) and time dependent-DFT (TD-DFT) calculations.

EXPERIMENTAL SECTION

Materials. The precursors pyrrole, *p*-chloranil, 2,4,5-trimethoxybenzaldehyde, and tetrabutyl ammonium perchlorate (TBAP) were purchased from Aldrich, USA. 4-Cyano benzaldehyde, 4-bromo benzaldehyde, and $FeCl_2{\cdot}4H_2O$ were purchased from Merck, India. Other chemicals were of reagent grade. Hexane and CH_2Cl_2 were distilled from KOH and CaH_2 respectively. For spectroscopy and electrochemical studies, HPLC-grade solvents were used. Symmetric A_3-corrole **1A** was obtained by following a literature reported procedure;[9,10] however, two *trans*-A_2B-corroles **2A** and **3A** have been prepared for the first time.

Physical Measurements. UV−Vis spectral studies were performed on a Perkin−Elmer LAMBDA-750 spectrophotometer. The elemental analyses were carried out with a Perkin−Elmer 240C elemental analyzer. FT−IR spectra were recorded on a Perkin−Elmer spectrophotometer with samples prepared as KBr pellets. The NMR measurements were carried out using a Bruker AVANCE 400 NMR spectrometer. Tetramethylsilane (TMS) was the internal standard. Electrospray mass spectra were recorded on a Bruker Micro TOF-QII mass spectrometer. Cyclic voltammetry measurements were carried out using a CH Instruments model CHI1120A electrochemistry system. A glassy carbon working electrode, a platinum wire as an auxiliary electrode, and an Ag-AgCl reference electrode were used in a three-electrode configuration. Tetrabutyl ammonium perchlorate (TBAP) was the supporting electrolyte (0.1 M), and the concentration of the solution was 10^{-3} M with respect to the complex. The half wave potential E^0_{298} was set equal to 0.5 (E_{pa} + E_{pc}), where E_{pa} and E_{pc} are anodic and cathodic cyclic voltammetric peak potentials, respectively. The scan rate used was 100 mV s^{-1}. The EPR spectra in the X band were recorded with a Bruker System EMX. Simulations of EPR spectra were done using the Simfonia program. UV−vis-NIR absorption spectra were recorded on an Avantes spectrometer system: Ava Light-DH-BAL (light source), AvaSpec-ULS2048 (UV−vis-detector), and AvaSpec-NIR256−2.5TEC (NIR-detector). Spectroelectrochemical measurements were carried out using an optically transparent thin layer electrochemical (OTTLE) cell.[11]

Crystal Structure Determination. Single crystals of **1B** were grown by slow diffusion of a solution of the **1B** in dichloromethane into methanol, followed by slow evaporation under atmospheric conditions, and those for **2B** were grown by slow diffusion of a solution of the (cor){FeNO}^{6} in dichloromethane into benzene, followed by slow evaporation under atmospheric conditions. The crystal data of **1B** and **2B** were collected on a Bruker Kappa APEX II CCD diffractometer at 293 K. Selected data collection parameters and other crystallographic results are summarized in Table S1, Supporting Information. All data were corrected for Lorentz polarization and absorption effects. The program package SHELXTL[12] was used for structure solution and full matrix least-squares refinement on F^2. Hydrogen atoms were included in the refinement using the riding model. Contributions of H atoms for the water molecules were included but were not fixed. Disordered solvent molecules were taken out using the SQUEEZE[13] command in PLATON.

CCDC-959930 and CCDC-959931 contain the supplementary crystallographic data for **1B** and **2B**. These data can be obtained free of charge via www.ccdc.cam.ac.uk/data_request/cif.

Computational Details. Full geometry optimizations were carried out using the DFT method at the (U)B3LYP level for $2B^+$ and $2B^-$ and (R)B3LYP for **2B**.[14] All elements except iron were assigned the 6-31G(d) basis set. The SDD basis set with effective core potential was employed for the iron atom.[15] Harmonic frequency calculations were performed on the optimized geometries, representing a minimum on the potential energy surface. All harmonic frequencies were corrected by a scaling factor of 0.975 except ν(NO), which was scaled by a factor of 0.92. All calculations were performed with the Gaussian09 program package.[16] Vertical electronic excitations based on B3LYP optimized geometries were computed for $2B^+$, **2B**, and $2B^-$ using the TD-DFT formalism[17] in dichloromethane using the conductor-like polarizable continuum model (CPCM).[18] *Chemissian*[19] was used to calculate the fractional contributions of various groups to each molecular orbital. All the calculated structures were visualized with *ChemCraft*.[20]

Synthesis of 4-(Di(1H-pyrrol-2-yl)methyl)benzonitrile, 1. 4-(Di(1H-pyrrol-2-yl)methyl)benzonitrile **1** was prepared by slight modification of the direct synthesis method reported by Lee et al., involving the pyrrole-aldehyde condensation in the presence of a large excess of pyrrole.[21] Pyrrole served a dual role of reactant and solvent in the reaction mixture. In a 100 mL two-necked round-bottomed flask, 2 g of 4-cyano benzaldehyde (0.015 mmol) was dissolved in 21 mL of pyrrole (0.300 mmol) and, after 233 μL (0.003 mmol) of TFA was added, was stirred for 20 min at room temperature. The brown-colored crude product was obtained after dilution with CH_2Cl_2, washing with dilute NaOH solution, and concentration of the organic layer. Excess pyrrole was removed by rotary evaporation. The crude product was then purified by column chromatography through a bed of silica-gel (100−200 mesh), using the solvent mixture 85% hexane and 15% ethylacetate as eluent.

For 4-(Di(1H-pyrrol-2-yl)methyl)benzonitrile, 1. The compound 4-(di(1H-pyrrol-2-yl)methyl)benzonitrile was characterized by various spectral techniques, such as CHN analysis, UV−vis, ^{1}H NMR, ^{13}C NMR, and electrospray mass spectrum. These analyses matched well with the earlier reported values.[21]

Synthesis of 5,10,15-Tris(4-bromophenyl)corrole, 1A. **1A** was prepared according to available procedures of corrole synthesis.[9] A total of 0.925 g of 4-bromo benzaldehyde (5 mmol) and 697 μL of pyrrole (10 mmol) were dissolved in 200 mL of methanol, and subsequently 200 mL of water was added. Then 4.25 mL of HCl_{aq} (36%) was added, and the reaction was stirred for 3 h. The mixture was extracted with $CHCl_3$, and the organic layer was washed twice with water, dried by anhydrous Na_2SO_4, filtered, and diluted to 300 mL with $CHCl_3$. A total of 1.23 g of *p*-chloranil (5 mmol) was added, and the mixture was refluxed for 1 h. The solvent was removed by rotary evaporation, and the green-colored crude product was purified by column chromatography through silica gel (100−200 mesh) bed and using 20% DCM and 80% hexane as eluent.

For 5,10,15-Tris(4-bromophenyl)corrole, 1A. The compound **1A** was characterized by various spectral techniques, such as CHN analysis, UV−vis, ^{1}H NMR, ^{13}C NMR, and electrospray mass spectrum, which also confirmed the purity and identity of **1A**. These analyses matched well with the earlier reported values.[10]

Synthesis of 10-(4-Bromophenyl)-5,15-bis(4-cyanophenyl)-corrole, 2A. **2A** was prepared by following a general procedure of corrole synthesis.[9] A total of 0.247 g of 5-(4-cyanophenyl)-dipyrromethane (1 mmol) and 0.092 g of 4-bromo benzaldehyde (0.5 mmol) were dissolved in 50 mL of MeOH. The reaction was kept for stirring for 1 h. The mixture was extracted with $CHCl_3$, and the organic layer was washed twice with H_2O, dried by anhydrous Na_2SO_4, filtered, and diluted to 250 mL with $CHCl_3$. Then, 0.369 g (1.5 mmol) of *p*-chloranil was added, and the mixture was refluxed for 1 h. The solvent was removed by rotary evaporation, and the green-colored crude product was purified by column chromatography through silica gel (100−200 mesh) column and using 80% DCM and 20% hexane as eluent.

For 10-(4-Bromophenyl)-5,15-bis(4-cyanophenyl)corrole, 2A. Yield: 45% (150 mg). Anal. calcd (found) for $C_{39}H_{23}BrN_6$ (**2A**): C, 71.45 (71.53); H, 3.54 (3.46); N, 12.82 (12.75). λ_{max}/nm (ε/M^{-1} cm^{-1}) in dichloromethane: 425 (100488), 582 (16544), 623

dx.doi.org/10.1021/ic402304e | Inorg. Chem. 2014, 53, 1417−1429

Scheme 2. Representative Synthesis of 2B

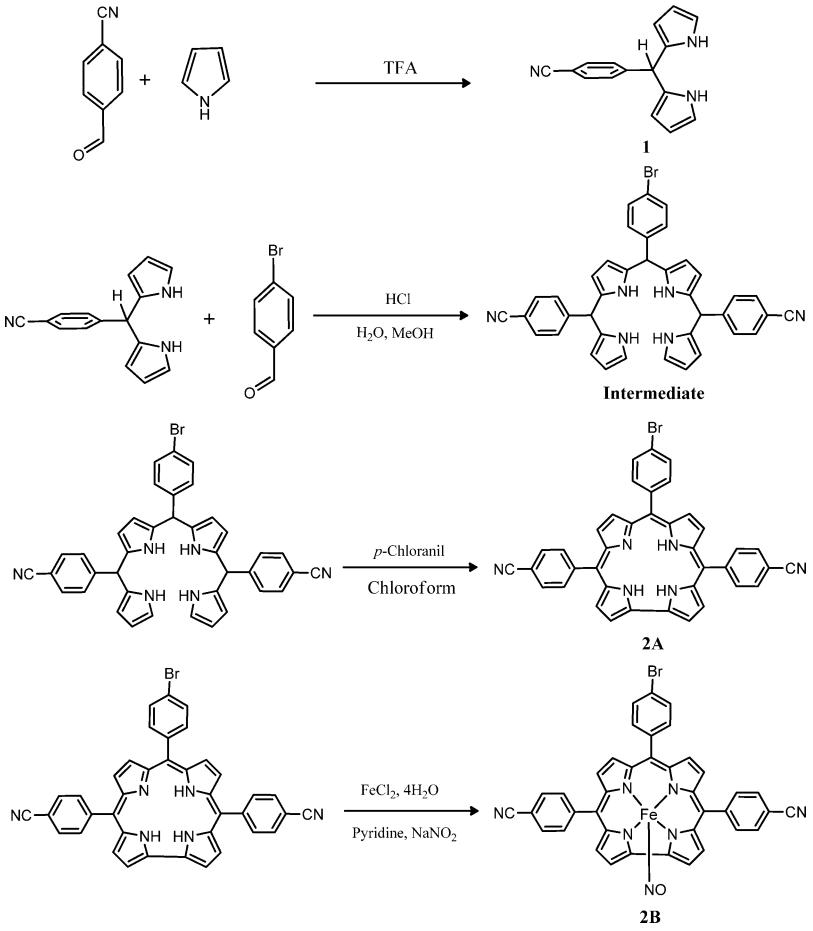

(11766), 648 (9409). ^{1}H NMR (400 MHz, $CDCl_3$) δ 9.063 (broad singlet, 2H), 8.854 (broad singlet, 2H), 8.611−8.486 (broad multiplet, 8H), 8.130−8.036 (broad multiplet, 6H), 7.922 (broad singlet, 2H). The electrospray mass spectrum in acetonitrile (see Supporting Information, Figure S1) showed peaks centered at m/z = 656.724 correspond to $[\mathbf{2A} + \mathbf{H}]^+$ (calculated molecular mass: 655.544).

Synthesis of 10-(2,4,5-Trimethoxyphenyl)-5,15-bis(4-cyanophenyl)corrole, 3A. **3A** was prepared by following a general procedure of corrole synthesis.[9] 0.247 g of 5-(4-cyanophenyl)-dipyrromethane (1 mmol) and 0.098 g of 2,4,5-trimethoxy benzaldehyde (0.5 mmol) were dissolved in 50 mL of MeOH. The reaction was kept for stirring for 1 h. The mixture was extracted with $CHCl_3$, and the organic layer was washed twice with H_2O, dried by anhydrous Na_2SO_4, filtered, and diluted to 250 mL with $CHCl_3$. Then, 0.369 g (1.5 mmol) of *p*-chloranil was added, and the mixture was refluxed for 1 h. The solvent was removed by rotary evaporation, and the green-colored crude product was purified by column chromatography through silica gel (100−200 mesh) column and using 80% DCM and 20% hexane as eluent.

For 10-(2,4,5-Trimethoxyphenyl)-5,15-bis(4-cyanophenyl)-corrole, 3A. Yield: 42% (140 mg). Anal. Calcd (found) for $C_{42}H_{30}N_6O_3$ (**3A**): C, 75.66 (75.53); H, 4.54 (4.46); N, 12.60 (12.75). λ_{max}/nm (ε/M^{-1} cm^{-1}) in dichloromethane: 426 (90875), 582 (17250), 627 (13000), 646 (11250). ^{1}H NMR (400 MHz, $CDCl_3$) δ 8.91 (s, 2H), 8.79 (s, 2H), 8.62 (s, 2H), 8.47 (s, 2H), 8.40 (d, J = 6.4 Hz, 4H), 8.05 (d, J = 6.7 Hz, 4H), 7.55 (s, 1H), 7.02 (s, 1H), 4.22 (s, 3H), 3.95 (s, 3H), 3.62 (s, 3H), −(1.37−1.43) (broad multiplet, 3H) (see Supporting Information, Figure S2). ^{13}C NMR (101 MHz, $CDCl_3$) δ 154.04, 150.28, 144.32, 142.53, 141.43, 139.11, 135.43, 132.12, 131.81, 126.86, 126.47, 122.52, 121.94, 119.43, 119.28, 116.78, 113.35, 111.05, 107.12, 98.17, 57.22, 56.86, 56.55 (see Supporting Information, Figure S3). The electrospray mass spectrum in acetonitrile (see Supporting Information, Figure S4) showed peaks centered at m/z = 667.21 corresponding to $[\mathbf{3A} + \mathbf{H}]^+$ (calculated molecular mass: 666.23). **3A** displayed strong fluorescence at 678 nm (see Supporting Information, Figure S5).

Synthesis of {5,10,15-Tris(4-bromophenyl)cor}Fe^{III}NO, 1B. A mixture of 0.025 g of 5,10,15-tris(4-bromophenyl)corrole (0.03 mmol) and 0.060 g of ferrous chloride tetrahydrate $FeCl_2{\cdot}4H_2O$ (0.3 mmol) was refluxed in a solution of 15 mL of pyridine/methanol (1:2) for 1-$^1/_2$ h under dinitrogen. A 1.0 mL aliquot of saturated aqueous $NaNO_2$ was then added to the hot solution, and the system was refluxed for an additional 30 min. The solution was then allowed to cool to room temperature, and the solvent mixture was removed by rotary evaporation. The solid product was finally dissolved in dichloromethane and purified by column chromatography using silica gel (100−200 mesh). The solvent-mixture used for elution of **1B** was 20% DCM and 80% hexane. The final form of the compound was obtained as orange-red crystalline materials.

For {5,10,15-Tris(4-bromophenyl)cor}Fe^{III}NO, 1B. Anal. Calcd (found) for $C_{37}H_{20}Br_3FeN_5O$ (**1B**): C, 52.52 (52.48); H, 2.38 (2.54); N, 8.28 (8.35). λ_{max}/nm (ε/M^{-1} cm^{-1}) in dichloromethane: 394(84800), 535(9400). $\nu_{N\equiv O}$ = 1773 cm^{-1}. ^{1}H NMR (400 MHz, $CDCl_3$) δ 7.98 (d, J = 4.6 Hz, 2H), 7.76−7.62 (m, 13H), 7.54 − 7.50 (m, 3H), 7.38 (d, J = 4.8 Hz, 2H). ^{13}C NMR (101 MHz, $CDCl_3$) δ 148.12, 147.91, 146.09, 138.46, 138.31, 137.35, 132.21, 132.01, 131.74, 131.69, 131.56, 131.53, 131.32, 130.44, 126.72, 126.02, 125.58, 123.13, 122.95, 118.49. The electrospray mass spectrum in acetonitrile matched well with the earlier reported data.[7d]

Synthesis of {10-(4-Bromophenyl)-5,15-bis(4-cyanophenyl)-cor}Fe^{III}NO, 2B. A mixture of 0.050 g of 10-(4-bromophenyl)-5,15-bis(4-cyanophenyl)corrole (0.076 mmol) and 0.152 g of ferrous chloride tetrahydrate $FeCl_2{\cdot}4H_2O$ (0.76 mmol) was refluxed in a solution of 15 mL of pyridine/methanol (1:2) for 1-$^1/_2$ h under

dx.doi.org/10.1021/ic402304e | *Inorg. Chem.* 2014, 53, 1417−1429

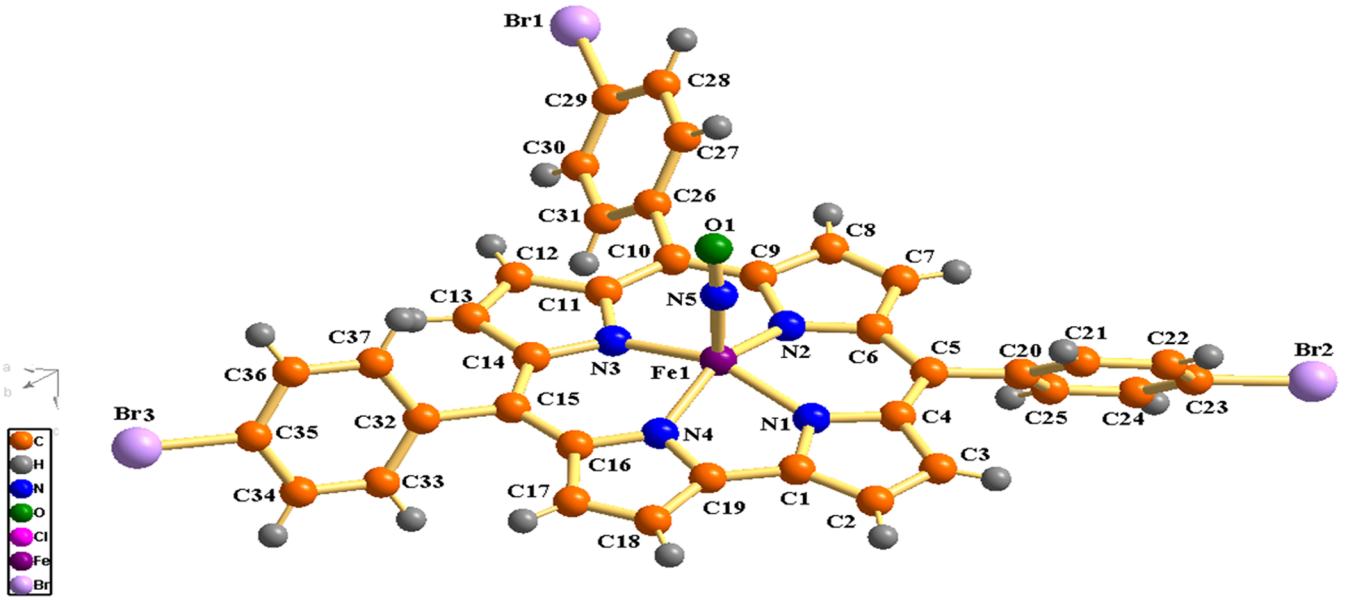

Figure 1. Single-crystal X-ray structure of **1B**.

dinitrogen. A 1.0 mL aliquot of saturated aqueous $NaNO_2$ was then added to the hot solution, and the system was refluxed for an additional 30 min. The solution was then allowed to cool to room temperature, and the solvent mixture was removed by rotary evaporation. The solid product was finally dissolved in dichloromethane and purified by column chromatography using silica gel (100−200 mesh). The solvent-mixture used for elution of **2B** was 60% DCM and 40% hexane. The final form of the compound was obtained as orange-red crystalline materials.

For {10-(4-Bromophenyl)-5,15-bis(4-cyanophenyl)cor]-Fe^{III}NO, 2B. Yield: 55% (31 mg). Anal. Calcd (found) for $C_{39}H_{20}BrFeN_7O$ (**2B**): C, 63.44 (63.48); H, 2.73 (2.84); N, 13.28 (13.40). λ_{max}/nm (ε/M^{-1} cm^{-1}) in dichloromethane: 390(56200), 539 (5000). $\nu_{N\equiv O}$ = 1774 cm^{-1}. ^{1}H NMR (400 MHz, $CDCl_3$) δ 8.04 (d, J = 4.6 Hz, 2H), 7.96−7.90 (m, 8H), 7.76−7.63 (m, 5H), 7.53−7.48 (m, 3H), 7.44−7.43(d, J = 5.0 Hz, 2H). ^{13}C NMR (101 MHz, $CDCl_3$) δ 148.14, 147.38, 146.09, 143.12, 138.18, 137.98, 132.24, 131.89, 131.68, 131.64, 131.62, 131.58, 131.35, 129.30, 126.37, 126.00, 125.81, 123.13, 119.08, 118.76, 112.68. The electrospray mass spectrum in acetonitrile (see Supporting Information, Figure S6) showed peaks centered at m/z = 709.308 corresponding to [M^+ − NO] (calculated molecular mass: 708.365).

Synthesis of {10-(2,4,5-Trimethoxyphenyl)-5,15-bis(4-cyanophenyl)cor}Fe^{III}NO, 3B. A mixture of 0.050 mg of 10-(2,4,5-trimethoxyphenyl)-5,15-bis(4-cyanophenyl)corrole (0.075 mmol) and 0.149 g of ferrous chloride tetrahydrate $FeCl_2{\cdot}4H_2O$ (0.75 mmol) was refluxed in a solution of 15 mL of pyridine/methanol (1:2) for 11/2 h under dinitrogen. A 1.0 mL aliquot of saturated aqueous $NaNO_2$ was then added to the hot solution, and the system was refluxed for an additional 30 min. The solution was then allowed to cool to room temperature, and the solvent mixture was removed by rotary evaporation. The solid product was finally dissolved in dichloromethane and purified by column chromatography using silica gel (100−200 mesh). The solvent used for elution of **3B** was 100% DCM. The final form of the compound was obtained as orange-red crystalline materials.

For {10-(2,4,5-Trimethoxyphenyl)-5,15-bis(4-cyanophenyl)-cor}Fe^{III}NO, 3B. Yield: 51% (29 mg). Anal. Calcd (found) for $C_{42}H_{27}FeN_7O_4$ (**3B**): C, 67.30 (67.48); H, 3.63 (3.74); N, 13.08 (12.95). λ_{max}/nm (ε/M^{-1} cm^{-1}) in dichloromethane: 388 (96200), 485 (25800). $\nu_{N\equiv O}$ = 1772 cm^{-1}. ^{1}H NMR (400 MHz, DMSO-d_6) δ 8.17−8.03 (m, 10H), 7.68−7.64 (dd, J = 9.6, 4.5 Hz, 2H), 7.42−7.40 (dd, J = 4.6, 3.2 Hz, 2H), 7.33−7.31 (t, J = 5.3 Hz, 2H), 7.09−6.93 (m, 2H), 3.93 (d, J = 2.9 Hz, 3H), 3.74 (s, 2H), 3.66 (d, J = 4.8 Hz, 2H), 3.55 (s, 2H). ^{13}C NMR (101 MHz, DMSO) δ 151.08, 150.92, 149.93, 149.90, 147.40, 147.38, 146.45, 146.37, 146.34, 142.06, 141.99, 141.69, 137.28, 132.15, 130.76, 130.09, 130.03, 129.43, 129.39, 128.81, 127.11, 126.05, 125.88, 125.83, 125.54, 125.48, 119.07, 118.40, 117.31, 117.23, 114.54, 114.12, 111.35, 98.44, 98.17, 56.38, 56.00, 55.51. The electrospray mass spectrum in acetonitrile (Figure S7, Supporting Information) showed peaks centered at m/z = 719.09 corresponding to [M^+ − NO] (calculated molecular mass: 719.14).

RESULTS AND DISCUSSION

Synthesis and Characterization. Symmetric A_3-corrole **1A** was already reported in the literature;[9,10] however, two *trans*-A_2B-corroles **2A** and **3A** were prepared for the first time. Reaction of the respective aryl-aldehydes and pyrrole, which were dissolved in a 1:1 mixture of methanol and water in the presence of HCl, and the subsequent oxidation by *p*-chloranil (Scheme 2; representative synthesis of **2B**), resulted in the formation of the corrole derivatives.

The [(cor){FeNO}^{6}] derivatives were synthesized by following a reported procedure.[7] A mixture of the desired corrole and ferrous chloride tetrahydrate was refluxed in a solution of pyridine/methanol (1:2) under a dinitrogen atmosphere. Upon addition of a saturated aqueous $NaNO_2$ solution, the corresponding [(cor){FeNO}^{6}] derivatives **1B**, **2B**, and **3B** were formed. Purity and identity of the free base corroles and the corresponding [(cor){FeNO}^{6}] derivatives were demonstrated by their satisfactory elemental analyses (see Experimental Section), IR spectroscopy data (Figure S8 and Table S2, Supporting Information), and the electrospray mass spectra. The electrospray mass spectrum of **1B** in chloroform matched well with the earlier reported data.[7d] The electrospray mass spectrum of **2B** in acetonitrile (see Supporting Information, Figure S6) shows peaks centered at m/z = 709.308 corresponding to [M^+ − NO] (calculated molecular mass: 708.365). The electrospray mass spectrum of **3B** in acetonitrile (Figure S7, Supporting Information) showed peaks centered at m/z = 719.09 corresponding to [M^+ − NO] (calculated molecular mass: 719.14).

NMR Spectra. The ^{1}H NMR spectrum of **1B** exhibits sharp peaks in accordance with 20 partially overlapping aromatic protons in the region δ, 8.0−7.3 ppm (see Supporting

dx.doi.org/10.1021/ic402304e | Inorg. Chem. 2014, 53, 1417−1429

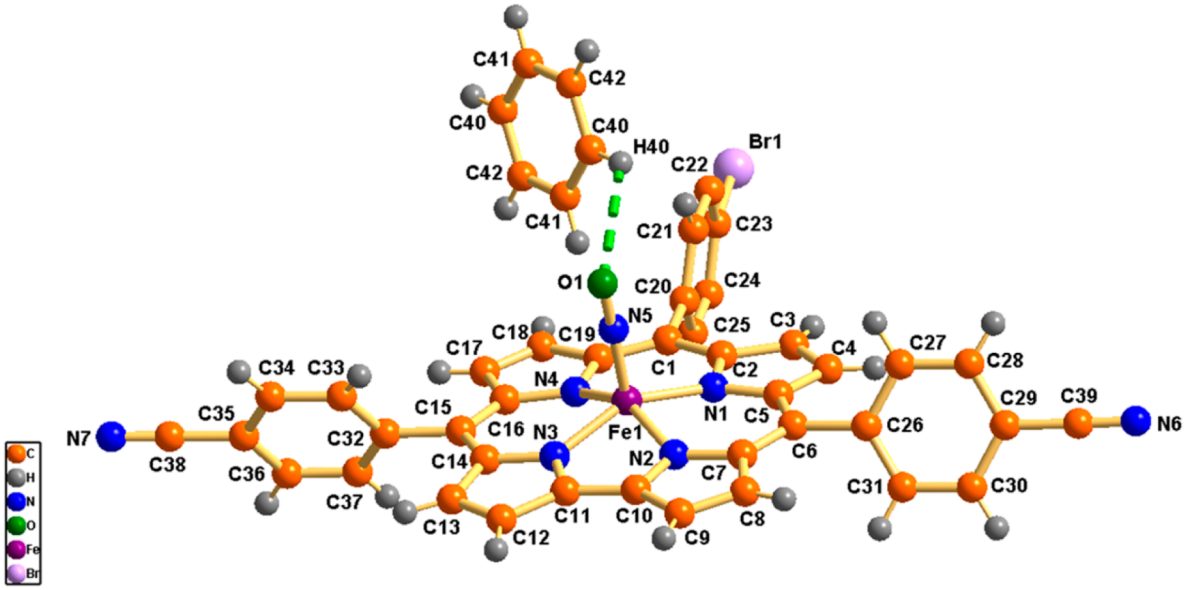

Figure 2. Single-crystal X-ray structure of **2B**.

Information, Figure S9). Out of these signals three doublets (δ = 7.98, 7.38, 7.53) are easily distinguishable with characteristic coupling constants J = ∼5.0 Hz. On the basis of earlier observations,[22] these doublets can be assigned to β-pyrrolic hydrogen atoms. Another doublet is overlapped with the aryl ring protons. The aryl ring protons are observed at the 7.76−7.50 ppm region. ^{13}C NMR spectrum shows the presence of the expected 20 signals (see Supporting Information, Figure S10). The ^{1}H NMR spectrum of **2B** exhibits the expected number of 20 partially overlapping aromatic protons in the region δ = 8.04−7.4 ppm (Figure S11, Supporting Information). Out of these signals, two doublets (δ = 8.04, 7.44) are easily distinguishable with characteristic coupling constants J = ∼5.0 Hz. These doublets are assigned as β-pyrrolic hydrogen atoms. Two more doublets are overlapped with the aryl ring protons. The aryl ring protons are observed at the 7.96−7.48 ppm region. ^{13}C NMR spectrum (see Supporting Information, Figure S12) shows the presence of the expected 21 signals. The ^{1}H NMR spectrum of **3B** shows sharp resonances corresponding to 18 partially overlapping aromatic protons in the region δ, 8.18−6.9 ppm (see Supporting Information, Figure S13). Nine methoxy protons appear in the region of 3.95−3.55 ppm. ^{13}C NMR spectrum (see Supporting Information, Figure S14) shows the presence of expected 38 signals due to complete asymmetric nature of the molecule. Out of those 38 signals, three methoxy group signals (δ = 56.38, 56.00, and 55.51) can be easily distinguished by their characteristic chemical shifts. All the signals in the [(cor){FeNO}^{6}] derivatives show an upfield shift compared to free base corroles. The ^{1}H and ^{13}C NMR data thus unequivocally establish the diamagnetic nature of the iron complexes **1B**−**3B**.

Crystal Structures. The crystal structures of **1B** and **2B** are shown in Figures 1 and 2, respectively. The crystal system is triclinic for **1B** and monoclinic for **2B**. The unit cell of **1B** contains two molecules and that of **2B** contains eight molecules. Important crystallographic parameters are presented in Table S1, Supporting Information. The DFT calculated bond distances and angles match fairly well with the experimental values for **2B** (Table 1). In **1B**, iron is penta-coordinated and surrounded by five nitrogen atoms. The geometry around the iron is distorted square pyramidal. The Fe−N distances are 1.9059(4), 1.929(4), 1.921(4), and 1.898(4) Å respectively and are typical for low-spin Fe (III). The N−Fe−N bond angles are 87.44(17)°, 93.18(18)°, 87.05(17)°, and 79.60(17)°. The Fe−N−O bond angle, 175.0(4)°, justifies calling it as a linear nitrosyl. The Fe−N (NO) bond distance, 1.656(4) Å, points toward a significant Fe^{III} → NO back bonding. The NO bond length, 1.159(5) Å, depicts its elongated character (Scheme 3 and Table 2). The iron atom is elevated from the peripheral 19-atom corrole carbon ring by 0.512(9) Å to give rise to a domed conformation. This leads to a consequent deviation of the pyrrole ring nitrogen atoms from the 19-atom corrole carbon ring by distances ranging from 0.018 to 0.140 Å. The *meso*-substituted phenyl rings are tilted with respect to the mean corrole plane (considered as the 19-atom corrole carbon ring) by dihedral angles ranging from 58.05−61.68°. In **2B**, iron is penta coordinated and surrounded by five nitrogen atoms. The geometry around the iron is distorted square pyramidal. Distance of Fe (III) from mean corrole plane is 0.516 (5) Å. The Fe−N distances are 1.919(3) (DFT: 1.927 Å), 1.895(2) (DFT: 1.902 Å), 1.889(3) (DFT: 1.901 Å), and 1.939(3) (DFT: 1.932 Å) Å (Table 1) and are typical for low-spin Fe(III). The N−Fe−N bond angles are 87.91(11)° (DFT: 87.72°), 79.06(12)° (DFT: 79.45°), 87.82(12)° (DFT: 87.59°), and 92.32(11)° (DFT: 93.10°) (Table 1). The Fe−N−O bond angle, 171.70(3)° (DFT: 179.94°) (Table 1), justifies calling it as a linear nitrosyl. The Fe−N(NO) bond distance, 1.650(3) Å (DFT: 1.597 Å) (Table 1), points toward a significant Fe^{III} → NO back bonding. The N−O bond length, 1.162(3) Å (DFT: 1.162 Å) (Table 1), depicts its elongated character.

Because of the square-pyramidal geometry around the central metal atom, the nitrogen atoms of the pyrrole rings in the macrocycle **2B** are alternately tilted up and down the mean corrole plane by a range of 0.0367−0.0873 Å. This prominent saddling effect in the corrole ring of **2B** is also consistent with the alternate deviation of the dihedral angles between the pyrrole rings with the mean corrole plane, which lie between 1.906−4.925°. The substituted phenyl rings at the *meso*-

dx.doi.org/10.1021/ic402304e | *Inorg. Chem.* 2014, 53, 1417−1429

Table 1. Selected X-ray and DFT Calculated (B3LYP/6-31G*/SDD) Bond Distances (Å) and Angles (deg) for 2B^n (n = 1+, 0, 1−)

	2B (X-ray)	2B (DFT) (S = 0)	2B$^+$ (DFT) (S = 1/2)	2B$^-$ (DFT) (S = 1/2)
Fe(1)−N(1)	1.919(3)	1.927	1.931	1.934
Fe(1)−N(2)	1.895(2)	1.902	1.918	1.911
Fe(1)−N(3)	1.889(3)	1.901	1.918	1.923
Fe(1)−N(4)	1.939(3)	1.932	1.970	1.962
Fe(1)−N(5)	1.650(3)	1.597	1.764	1.837
N(5)−O(1)	1.162(3)	1.162	1.174	1.196
N(1)−C(2)	1.389(4)	1.387	1.380	1.377
N(1)−C(5)	1.385(4)	1.387	1.371	1.386
N(2)−C(7)	1.386(4)	1.380	1.381	1.364
N(2)−C(10)	1.357(5)	1.366	1.344	1.372
N(3)−C(11)	1.357(4)	1.364	1.340	1.369
N(3)−C(14)	1.386(4)	1.377	1.380	1.361
N(4)−C(16)	1.383(4)	1.390	1.369	1.386
N(4)−C(19)	1.379(5)	1.390	1.380	1.376
C(1)−C(2)	1.404(4)	1.407	1.424	1.414
C(2)−C(3)	1.428(5)	1.434	1.430	1.440
C(3)−C(4)	1.354(5)	1.367	1.377	1.369
C(4)−C(5)	1.431(5)	1.436	1.428	1.441
C(5)−C(6)	1.423(5)	1.419	1.457	1.419
C(6)−C(7)	1.383(5)	1.397	1.390	1.418
C(7)−C(8)	1.437(5)	1.438	1.449	1.439
C(8)−C(9)	1.367(5)	1.381	1.378	1.388
C(9)−C(10)	1.428(5)	1.427	1.432	1.422
C(10)−C(11)	1.421(5)	1.415	1.456	1.420
C(11)−C(12)	1.428(5)	1.427	1.433	1.425
C(12)−C(13)	1.372(5)	1.381	1.377	1.386
C(13)−C(14)	1.433(5)	1.438	1.447	1.441
C(14)−C(15)	1.389(5)	1.398	1.393	1.418
C(15)−C(16)	1.414(5)	1.418	1.454	1.419
C(16)−C(17)	1.431(5)	1.436	1.431	1.441
C(17)−C(18)	1.352(6)	1.367	1.376	1.369
C(18)−C(19)	1.433(4)	1.434	1.431	1.440
C(19)−C(1)	1.398(5)	1.405	1.423	1.415
O(1)−N(5)−Fe(1)	171.70(3)	179.94	147.89	135.56
N(1)−Fe(1)−N(2)	87.91(11)	87.72	88.99	89.12
N(1)−Fe(1)−N(3)	152.50(12)	153.99	158.20	159.22
N(1)−Fe(1)−N(4)	92.32(11)	93.10	93.73	93.92
N(1)−Fe(1)−N(5)	105.45(13)	101.80	96.81	95.89
N(2)−Fe(1)−N(3)	79.06(12)	79.45	79.61	80.29
N(2)−Fe(1)−N(4)	150.94(11)	150.93	151.96	154.21
N(2)−Fe(1)−N(5)	101.25(13)	105.20	103.38	101.01
N(3)−Fe(1)−N(4)	87.82(12)	87.59	88.04	88.25
N(3)−Fe(1)−N(5)	100.81(14)	103.36	103.84	103.62
N(4)−Fe(1)−N(5)	106.66(12)	103.07	103.99	104.12

positions of the corrole rings are placed at angles varying from 65.04−80.54° with respect to the mean corrole plane.

The comparison of all these structural parameters involving **1B** and **2B** with those of the [(cor){FeNO}^{6}] derivatives reported by others[7] earlier clearly justifies the aforesaid discussions. In the packing diagram of both **1B** and **2B** between two neighboring molecules, NO groups are facing in opposite directions, and the planes of the rings are approximately parallel. For **1B** the interplanar distance between two corrole planes is ∼3.53 Å. The distance between two iron atoms is 7.0949(11) Å. For **2B**, the interplanar distance between two corrole planes is ∼4.63 Å. The distance between two iron atoms is 8.60(7) Å. The crystal structure analyses of both the compounds **1B** (see Supporting Information, Figures S15 and S17) and **2B** (see Supporting Information, Figures S16 and S18) show several C−H···N interactions, C−H···C interactions, C−H···O interactions, and C−H···π interactions. **1B** molecules are stacked together and form layer-like arrangements throughout the crystal lattice. Similarly, **2B** molecules are stacked together and form cylindrical tubelike arrangements throughout the crystal lattice. These tubes are filled with benzene molecules. Inside the tube, benzene molecules are interconnected through $\pi-\pi$ stacking interactions {see Supporting Information, Figure S16b}. The closest distance between two neighboring [(cor){FeNO}^{6}] molecules responsible for $\pi-\pi$ stacking interactions is ∼3.18 Å for **1B** and ∼3.32 Å for **2B**. This clearly indicates that there is a reasonably strong adjacent parallel plane $\pi-\pi$ stacking interaction between the [(cor){FeNO}^{6}] molecules. The shortest intermolecular distance between two [(cor){FeNO}^{6}] molecules responsible for C−H···O interactions, C−H···C interactions, C−H···N interactions, and C−H···π interactions are close to ∼2.71 Å, ∼2.85 Å, ∼3.01 Å, and 2.75−4.04 Å respectively for **1B** and ∼2.69 Å, ∼2.89 Å, ∼2.85 Å, and 2.89−3.47 Å respectively for **2B**. This is quite clearly indicative of the fact that fairly strong intermolecular C−H···π interactions, C−H···O, C−H···N, and C−H···C interactions are also present between adjacent [(cor){FeNO}^{6}] molecules. It has been assumed that the solid state structures are stable due to intermolecular parallel-displaced $\pi-\pi$ stacking interactions, C−H···π interactions, C−H···O, C−H···N, and C−H···C interactions.[23]

Redox Properties of the 1B, 2B, and 3B. The redox properties of the **1B**, **2B**, and **3B** were investigated in CH_2Cl_2/0.1 M TBAP (TBAP = tetra-*n*-butyl ammonium perchlorate) by using cyclic voltammetric techniques and differential pulse voltammetric techniques (Figure 3 and Table 3). The oxidation processes at the positive side of Ag-AgCl reference electrode were recorded by using a platinum working electrode; a glassy−carbon working electrode was used for recording the reduction processes. All the three iron complexes **1B**, **2B**, and **3B** exhibited one reversible oxidative couple E^0_{298}, V (ΔE_p, mV): +0.54 (70) (**1B**), +0.58 (70) (**2B**), and +0.56(70) (**3B**) versus ferrocene/ferrocenium. They also showed one reversible reductive couple E^0_{298}, V (ΔE_p, mV): −0.67(70) (**1B**), −0.61(70) (**2B**), and −0.63(70) (**3B**) versus ferrocene/ferrocenium. The effect of the substituents in the corrolato ring on the redox potentials of the metal complexes is marginal. UV−vis, IR, and EPR spectroelectrochemical investigations were done on both the oxidative couple and reductive couple to gain insights into the electronic structures of the various states.

UV−vis, IR, and EPR Spectroelectrochemistry. Electronic spectral data of the compounds in CH_2Cl_2 (see Supporting Information, Figure S19) are shown in Table S2 (see Supporting Information). All the three complexes **1B**, **2B**, and **3B** exhibit Soret bands in the range of 385−395 nm. Another weak band in the range of 485−540 nm is observed in the visible region.[7] The molar absorption coefficient of the Soret bands is in the range of (5.6−9.6) × 10^4 M^{-1} cm^{-1}, and the molar absorption coefficient of the bands in the visible region is in the range of (5.0−26.0) × 10^3 M^{-1} cm^{-1}. Spectroelectrochemical measurements (UV−vis, FT-IR, and EPR) of all the nitrosyl derivatives were carried out in dichloromethane solvent at room temperature. These measurements were carried out to find the characteristic spectroscopic changes involved in all the accessible redox states of the

dx.doi.org/10.1021/ic402304e | Inorg. Chem. 2014, 53, 1417−1429

Scheme 3. Structural Parameters of 1B and 2B

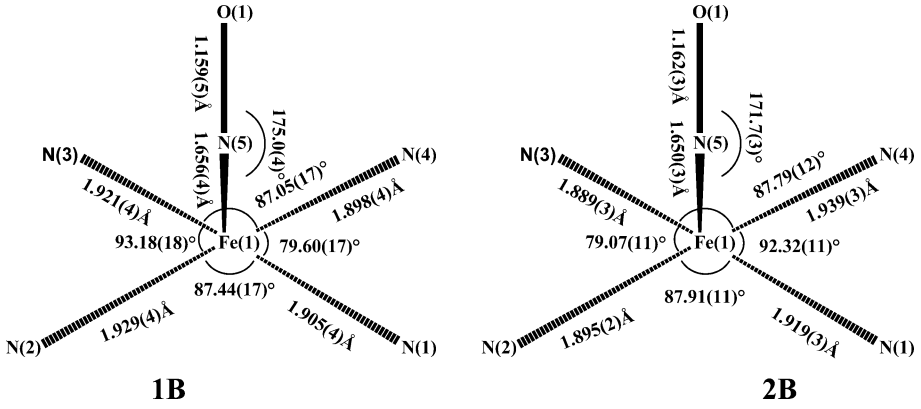

Table 2. Comparison of Structural Parameters and NO Stretching Frequencies of (cor){FeNO}^{6} Species Having Electronic Configuration of {FeNO}^{6} Already Available in the Literature with 1B and 2B

compound[a]	Fe−NO bond distance (Å)	N−O bond distance (Å)	Fe−N−O bond angle (deg)	NO stretching freq (cm^{-1})	ref
(OEC)Fe(NO)	1.631(3)	1.171(4)	176.9(3)	1767	7a
(TMOPC)Fe(NO)	1.702(4)	1.076(4)	172.0(4)	1767	7d
(TTC)Fe(NO)	1.645(2)	1.162(2)	177.1(2)	1761	7d
(TDCC)Fe(NO)	1.641(4)	1.169(5)	172.3(4)	1783	7f
(TF_5PC)Fe(NO)	1.639(4)[b], 1.648(4)	1.166(4), 1.171(4)	177.3(4), 178.0(4)	1801	7f
(TNPC)Fe(NO)	1.675(14)[b] 1.648(11)	1.144(15), 1.154(13)	172.8(10), 173.3(9)	1778	7d, 7b
1B	1.656(4)	1.159(5)	175.0(4)	1773	this work
2B	1.650(3)	1.162(3)	171.7(3)	1774	this work

[a]OEC = octaethylcorrole, TMOPC = tris(*p*-methoxyphenyl)corrole, TTC = tris(*p*-methylphenyl)corrole, TDCC = tris(*o*-dichlorophenyl)corrole, TF_5PC = 5,10,15-tris(pentafluorophenyl)corrole, TNPC = 5,10,15-tris(4-nitrophenyl)corrole. [b]There are two crystallographically independent molecule exists in the asymmetric unit.

complexes and to establish the site of electron transfer in the nitrosyl derivatives. Furthermore, these measurements were also helpful in elucidating the reversibility of the redox processes. UV−vis, IR, and EPR spectroelectrochemical studies of all the three nitrosyl derivatives show similar pattern (Figures 4, 5, and 6). Hence, one representative example (complex **3B**) will be discussed here. For rest of the complexes, data are presented in a tabular form (Tables 4, 5, and 6). Complex **3B** shows its Soret and Q bands at 391, 532, and 631 nm respectively (Figure 4). On oxidation of **3B** to **3B**$^+$ in dichloromethane/0.1 M BuN_4PF_6 using an optically transparent thin layer (OTTLE) cell,[11] the Soret band at 391 nm loses intensity, and two new bands appear at 365 nm and 397 nm (Figure 4a and Table 4). The initial Q bands lose their intensity, and new bands appear at 500 and 635 nm. The shift of the Soret and Q bands to lower energies is consistent with earlier literature reports.[7a,b] Literature reports suggest that this kind of shifting of Soret and Q bands to lower energies is due to the formation of corrole radical cation or the formation of Fe(IV) corrole.[7a,b] On returning back to the initial potential, the native spectrum of **3B** was regained in band position and intensity to 100%, thus confirming the reversibility of the oxidation process. The FTIR thin-layer spectroelectrochemical measurement of one-electron oxidized species **3B**$^{\bullet+}$ in dichloromethane/0.1 M BuN_4PF_6 was also performed (Figure 5a and Table 5). The shift of the ν_{NO} stretching frequency on one-electron oxidation occurs from 1782 cm^{-1} to 1820 cm^{-1}, which corresponds to 38 cm^{-1}. This small shift is an indication of the {FeNO}^{6} unit remaining largely unaffected by the oxidation step, and the oxidation taking place on the corrolato ring. In order to get a direct proof of the location of the unpaired spin in the paramagnetic **3B**$^{\bullet+}$ form, EPR spectroscopy was performed on the electrogenerated **3B**$^{\bullet+}$ in solution. The X-band EPR spectrum of **3B**$^{\bullet+}$ at 295 K in CH_2Cl_2/0.1 M Bu_4NPF_6 displays an isotropic signal centered at g = 2.005 with a peak to peak separation of about 15 G (Figure 6a). The observation of the signal in fluid solution at 295 K, the closeness of the g-value to the free electron value of 2.0023, and the narrow line-width of only 15 G are a clear indication of the spin being predominantly localized on an organic ligand. The EPR result, taken together with the relatively small shift of the NO stretching frequency on moving from **3B** to **3B**$^{\bullet+}$ as observed in IR spectroelectrochemistry, convincingly proves the generation of a corrole based radical upon one-electron oxidation of **3B**. The one-electron oxidized form is thus best described as $[(cor)^{2\bullet-}\{FeNO\}^6]^{\bullet+}$. It should be noted here that the EPR spectrum of the one-electron oxidized forms of related (cor)FeNO complexes measured at 120 K have been described in terms of a low spin Fe(III) signal.[7a,b] For the present case, we have convincing data to prove the observation of a corrole radical signal by EPR spectroscopy. Since the literature reports also claim oxidation of the cor unit (from UV−vis and IR spectroscopic experiments), it remains unclear as to how the final EPR spectrum observed for the oxidized species originates from a low spin Fe(III) center. In the starting complexes $[(cor)^{3-}\{Fe(NO)\}^6]$, the {FeNO}^{6} units are clearly diamagnetic. An oxidation of the corrole unit will generate a species $[(cor)^{2\bullet-}\{Fe(NO)\}^6]^{\bullet+}$ which should logically possess a corrole centered spin. The only way to obtain a low spin Fe(III)-type EPR signal for the $[(cor)^{2\bullet-}\{Fe(NO)\}^6]$ form would be for the NO centered spin and the $(cor)^{2\bullet-}$ spin to couple antiferromagnetically, leaving a lone spin on Fe(III).

dx.doi.org/10.1021/ic402304e | *Inorg. Chem.* 2014, 53, 1417−1429

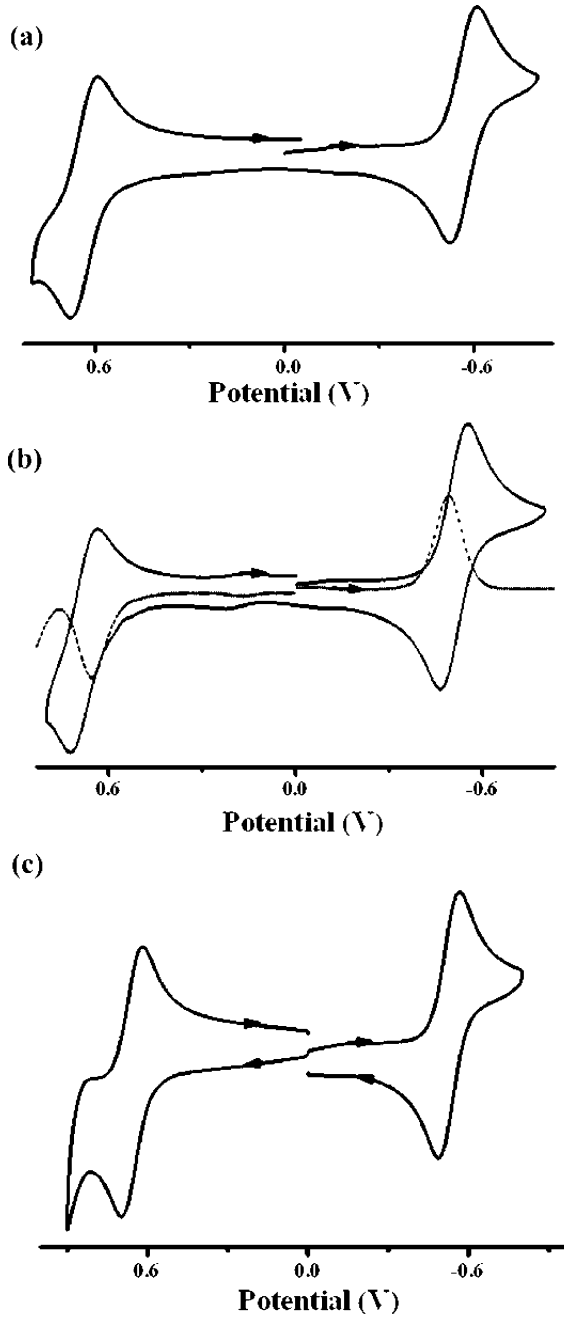

Figure 3. (a) Cyclic voltammograms of **1B** (—) in CH_2Cl_2 (b) cyclic voltammograms (—) and differential pulse voltammograms (---) of **2B** in CH_2Cl_2 and (c) cyclic voltammograms of **3B** (—) in CH_2Cl_2. The potentials are versus ferrocene/ferrocenium.

Table 3. Electrochemical Data[a]

	electrochemical data	
compound	oxidation E^0, V (ΔE_p, mV)	reduction E^0, V (ΔE_p, mV)
1B	0.54 (70)	−0.67(70)
2B	0.58 (70)	−0.61(70)
3B	0.56(70)	−0.63(70)

[a]In dichloromethane. The potentials are versus ferrocene/ferrocenium.

Considering the highly covalent nature of the Fe−NO bond, such a spin situation as stated above is unlikely. There are reports on the generation of porphyrin centered radicals on the

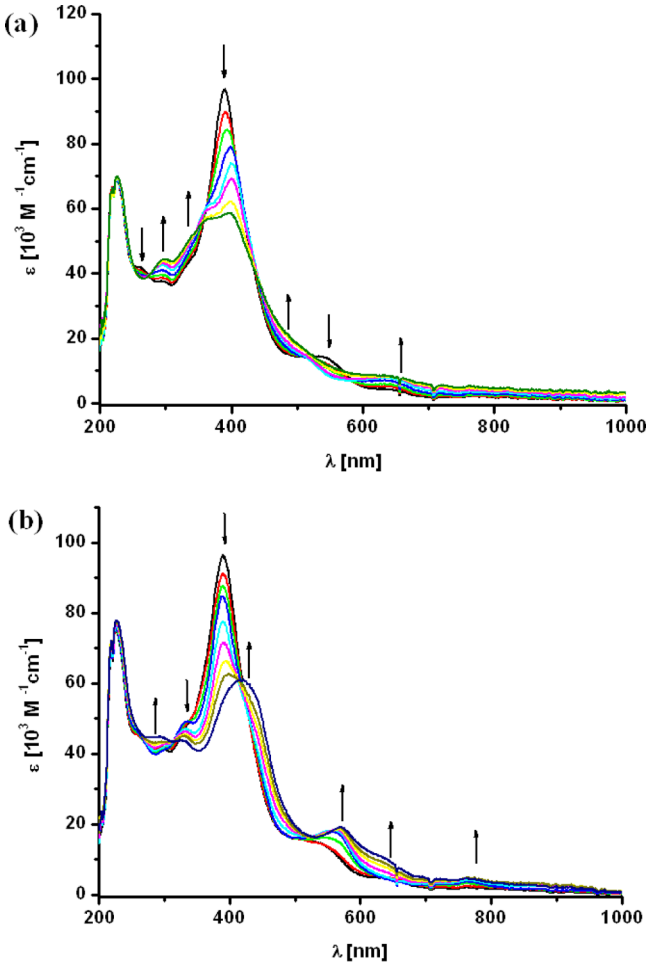

Figure 4. Changes in the UV−vis spectrum of **3B** (a) during first oxidation and (b) during first reduction. Results from OTTLE spectroelectrochemistry in CH_2Cl_2/0.1 M Bu_4NPF_6.

oxidation of similar nitrosyl containing metal complexes of porphyrin.[24]

On reduction of **3B** to $\mathbf{3B}^{\bullet-}$ in dichloromethane/0.1 M BuN_4PF_6 using an optically transparent thin layer electrochemical (OTTLE) cell, the Soret band at 391 nm loses its intensity and is shifted to 417 nm (Figure 4b). The initial Q bands show a reduced intensity, and three new bands appear at 571, 633, and 761 nm. The shift of the Soret and Q bands to lower energies is also supported by earlier literature reports.[7a,b] The FTIR thin-layer spectroelectrochemical measurement of one-electron reduced species, $\mathbf{3B}^{\bullet-}$ in dichloromethane/0.1 M BuN_4PF_6 was also performed (Figure 5b). The shift of the ν_{NO} stretching frequencies occurs from 1782 cm^{-1} to 1605 cm^{-1}, which corresponds to 177 cm^{-1}. As compared to the native state, the NO band is shifted to lower wavenumbers on reduction. On oxidation, this band shifts to higher wavenumbers (see below). This opposite trend is a result of the different charges induced on the complex on reduction and oxidation. The 177 cm^{-1} shift of the NO band to lower energies on reduction as compared to the native state is a direct indication that the {FeNO} unit is predominantly affected by this electron uptake. The IR results thus point to the formation of a complex $[(cor)^{3-}\{FeNO\}^7]^{\bullet-}$ on one-electron reduction, which contains a bent $\{FeNO\}^7$ unit. EPR spectroscopy of the one-electron reduced form further strengthens this assignment.

dx.doi.org/10.1021/ic402304e | Inorg. Chem. 2014, 53, 1417−1429

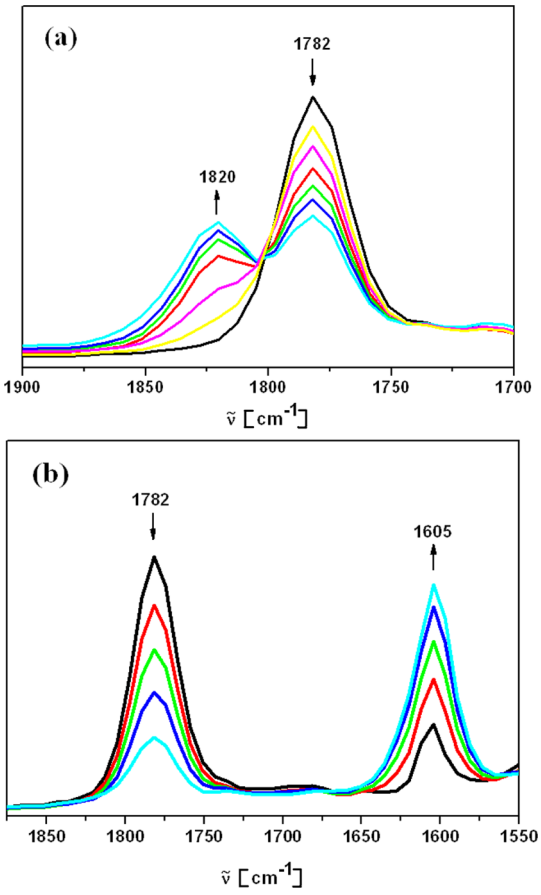

Figure 5. Changes in the IR spectrum of **3B** (a) during first oxidation and (b) during first reduction. Results from OTTLE spectroelectrochemistry in CH_2Cl_2/0.1 M Bu_4NPF_6.

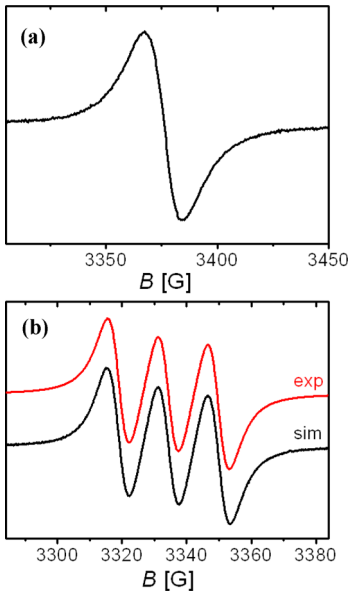

Figure 6. X-band EPR spectrum of (a) $\mathbf{3B}^{\bullet+}$ and (b) $\mathbf{3B}^{\bullet-}$ with simulation generated by in situ electrolysis at 295 K in CH_2Cl_2/0.1 M Bu_4NPF_6.

The in situ generated one-electron reduced species $\mathbf{3B}^{\bullet-}$ in CH_2Cl_2/0.1 M Bu_4NPF_6 at 295 K shows an isotropic signal centered at g = 2.029 in its X-band EPR spectrum.

Table 4. UV-Vis Data of $1B^n$, $2B^n$, and $3B^n$ [n = −1, +1, 0] from Spectroelectrochemistry[a]

complex	λ_{max} [nm] (ε [10^3 M^{-1} cm^{-1}])
$\mathbf{1B}^0$	225 (70.3); 272 sh; 396 (85.0); 514 sh; 627 (4.5)
$\mathbf{1B}^+$	225 (70.3); 283 sh; 361 (58.0); 416 (57.4); 510 sh; 641 (8.0); 882 (3.8)
$\mathbf{1B}^-$	225 (69.8); 282 sh; 333 (41.9); 404 (64.6); 565 (16.6); 629 sh; 761 (4.9)
$\mathbf{2B}^0$	225 (40.1); 262 (24.7); 332 sh; 390 (56.2); 533 (8.5)
$\mathbf{2B}^+$	226 (40.1); 265 sh; 339 sh; 360 sh; 399 (38.0); 497 sh; 637 (3.7)
$\mathbf{2B}^-$	224 (42.1); 261 sh; 330 (24.1); 399 sh; 422 (40.7); 570 (12.0); 633 (7.0); 765 (2.1)
$\mathbf{3B}^0$	226 (69.0); 260 sh; 296 sh; 333 sh; 391 (96.8); 532 (14.5); 631 (4.6)
$\mathbf{3B}^+$	227 (70.1); 297 (44.2); 365 sh; 397 (58.6); 500 sh; 635 (8.4)
$\mathbf{3B}^-$	227 (78.0); 293 (44.9); 325 (43.9); 417 (60.9); 571 (19.1); 633 sh; 761 (4.7)

[a]Measurements in CH_2Cl_2/0.1 M Bu_4NPF_6 (OTTLE spectroelectrochemistry).

Table 5. IR Data of $1B^n$, $2B^n$, and $3B^n$ [n = −1, +1, 0] from Spectroelectrochemistry[a]

complex	IR data[a] $\nu_{N\equiv O}$ (cm^{-1})
$\mathbf{1B}^0$	1779
$\mathbf{1B}^+$	1820
$\mathbf{1B}^-$	1606
$\mathbf{2B}^0$	1785
$\mathbf{2B}^+$	1825
$\mathbf{2B}^-$	1604
$\mathbf{3B}^0$	1782
$\mathbf{3B}^+$	1820
$\mathbf{3B}^-$	1605

[a]Measurements in CH_2Cl_2/0.1 M Bu_4NPF_6 (OTTLE spectroelectrochemistry).

Table 6. EPR Data[a] of Paramagnetic States[b]

complex	EPR data[a] (g)
$\mathbf{1B}^0$	
$\mathbf{1B}^+$	2.002
$\mathbf{1B}^-$	2.029; A(^{14}N) = 15.4 G
$\mathbf{2B}^0$	
$\mathbf{2B}^+$	2.003
$\mathbf{2B}^-$	2.029 A(^{14}N) = 15.5 G
$\mathbf{3B}^0$	
$\mathbf{3B}^+$	2.005
$\mathbf{3B}^-$	2.029 A(^{14}N) = 15.4 G

[a]g values measured at 295 K. [b]From EPR spectroelectrochemistry in CH_2Cl_2/0.1 M Bu_4NPF_6.

Furthermore, hyperfine coupling to one nitrogen nucleus (I = 1) is observed. The spectrum could be simulated with a a(N) value of 15.4 G. This signal is thus a direct proof of the spin being predominantly located in the {FeNO} part, and hence the EPR spectrum of $\mathbf{3B}^{\bullet-}$ corroborates its assignment as $[(cor)^{3-}\{FeNO\}^7]^{\bullet-}$ as has been stated above. Previous literature reports have drawn similar conclusions regarding the nature of the one-electron reduced form of such compounds.[7a,b]

The above observations have been supported by detailed theoretical investigations. The energy obtained on open shell singlet optimization is lower than that for a triplet configuration or closed shell singlet state of **2B**, which supports the

dx.doi.org/10.1021/ic402304e | Inorg. Chem. 2014, 53, 1417−1429

antiferromagnetic coupling between the unpaired spins on Fe(III) (d^5-low spin, t_{2g}^5) and NO$^\bullet$. The 99% contribution of cor to the HOMO of **2B** (Table S3, Supporting Information) indicates that oxidation occurs from the corrole moiety, which is further supported by the 95% and 96% contributions of cor to the α-SOMO and β-LUMO of **2B**$^+$ respectively (Table S4, Supporting Information). This is also reflected in the increase in Fe−N(cor) bond lengths and shortening of C−N(cor) bond distances on moving from **2B** to **2B**$^+$ as seen from their DFT optimized structures (Table 1, Figure S20, Supporting Information). A further support arises from the spin density distribution in **2B**$^+$ (Fe: 1.969, NO: −1.020, cor: 0.044; Table 7, Figure 7a) where an appreciable spin of 0.044 arises on the

Table 7. DFT Calculated (UB3LYP/6-31G*/SDD) Mulliken Spin Densities for 2B^n (n = 1+, 1−)

complex	Fe	NO	cor
2B$^+$ (S = 1/2)	1.969	−1.020	0.044
2B$^-$ (S = 1/2)	2.192	−1.202	0.012

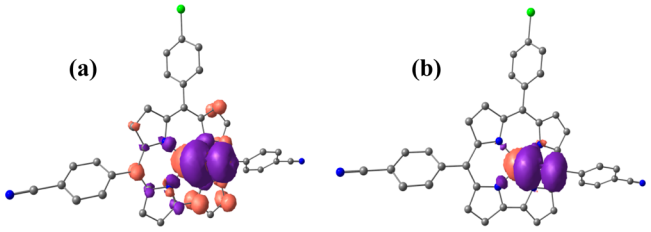

Figure 7. Spin density (UB3LYP/6-31G*/SDD) representations for (a) **2B**$^+$ and (b) **2B**$^-$.

corrole moiety unlike the absence of spin on it in **2B**. The fact that oxidation does not occur from NO is established by a negligible change in the ν(N−O) frequency ($\Delta\nu \approx 40$ cm^{-1}) on moving from **2B** (1785 cm^{-1} (exp) and 1778 cm^{-1} (DFT)) to **2B**$^+$ (1825 cm^{-1} (exp) and 1822 cm^{-1} (DFT)) (Table 8,

Table 8. IR Spectral Data (Experimental from Spectroelectrochemistry[a] and DFT[b]) for 2B^n (n = 1+, 0, 1−)

complex	$\nu_{(N-O)}$ (cm^{-1}) (exp)[a]	$\nu_{(N-O)}$ (cm^{-1}) (DFT)[b]
2B^0	1785	1778
2B$^+$	1825	1822
2B$^-$	1604	1613

[a]Measurements in CH_2Cl_2/0.1 M Bu_4NPF_6 (OTTLE spectroelectrochemistry) [b]B3LYP/6-31G*/SDD/CPCM/CH_2Cl_2.

Figure S21, Supporting Information). The 40%, 23%, and 38% contributions of Fe, NO, and cor to the HOMO of **2B** (Table S3) respectively collectively predict the possibility of reduction on any of the three moieties, although the α-SOMO and β-HOMO of **2B**$^-$ having 76% and 96% contributions from cor respectively (Table S5, Supporting Information) predict the reduction taking place at the corrole moiety. The spin density distribution in **2B**$^-$ of Fe: 2.192, NO: −1.202 and cor: 0.012 shows appreciable amount of spin residing on the Fe and NO (Table 7, Figure 7b). Moreover, the appreciable lengthening of the N−O bond from 1.162 Å in **2B** to 1.196 Å in **2B**$^-$ (Table 1) predicts that the reduction occurs at the NO. This is further supported by the ∼180 cm^{-1} decrease in the ν(N−O) frequency on moving from **2B** (1785 cm^{-1} (exp) and 1778 cm^{-1} (DFT)) to **2B**$^-$ (1604 cm^{-1} (exp) and 1613 cm^{-1} (DFT)) (Table 8, Figure S21, Supporting Information). These DFT results showing the occurrence of reduction predominantly at NO are further proven by the experimentally obtained triplet EPR showing the hyperfine splitting due to the I = 1 nuclear spin on ^{14}N, which interacts with the spin of the unpaired electron on the NO. The experimentally obtained UV−Vis transitions of native species **2B**, one-electron oxidized species **2B**$^+$, and one-electron reduced species **2B**$^-$ are in good agreement with the computed values (Table 9). For instance, **2B** displays intense ligand-to-ligand charge transfer (LLCT) transitions in the UV region (cor(π) → cor(π^*) at 225 and 262 nm) (Table 9). The visible region transitions at 390 and 533 nm arise due to ligand-to-metal charge transfer (LMCT) transition (cor(π) → Fe(dπ)) (Table 9). The one-electron oxidized species **2B**$^+$ exhibits LLCT transitions (cor(π) → cor(π^*)) at 399 and 637 nm (Table 9). The one-electron reduced species **2B**$^-$ shows metal-to-ligand charge transfer (MLCT) transition (Fe(dπ) → cor(π^*)) in the UV region at 330 nm (Table 9). In the visible region, it displays LLCT bands at 422 nm (NO(π)/cor(π) → cor(π^*)), 422, 570, 633, and 765 nm (cor(π) → cor(π^*)) (Table 9).

CONCLUSIONS

We have presented here the synthesis of two new corrole ligands. These new, and a literature reported corrole, have been used to generate a series of [(cor){FeNO}^{6}] derivatives. Purity and identity of the free base corroles and the corresponding [(cor){FeNO}^{6}] derivatives have been demonstrated by various spectroscopic techniques and elemental analysis. The ^{1}H NMR spectra of the [(cor){FeNO}^{6}] derivatives show sharp resonances, which indicate their diamagnetic characteristics and the noninnocent nature of the corrole macrocycles. The Fe−N−O bond angle is 175.0(4)° for **1B** and 171.7(3)° for **2B**. This indicates that these are linear nitrosyls of the {FeNO}^{6} form. In the packing diagram, **2B** molecules are stacked together and form cylindrical tubelike arrangements throughout the crystal lattice. These tubes are filled with benzene molecules, arranged as benzene clusters. All the three [(cor){FeNO}^{6}] derivatives **1B**, **2B**, and **3B** exhibited one reversible oxidative couple and one reversible reductive couple versus ferrocene/ferrocenium. UV−vis, IR, and EPR spectroelectrochemical measurements of one-electron oxidized species supports the formation of [(cor)$^{2\bullet-}${Fe(NO)}^{6}]$^{\bullet+}$. From earlier observations, it was established that EPR signals predominantly originate from a low spin Fe(III) center. However, our observations clearly prove the predominant location of the spin on the corrole unit. A rationale also has been provided for this. Thus, the EPR data point toward a new/alternative assignment of corrolato-iron-nitrosyl radical cation. UV−vis, IR, and EPR spectroelectrochemical studies of the reduced form **3B**$^{\bullet-}$ indicate that the unpaired electron in that species resides predominantly on the {FeNO} unit. The above observations have been supported by DFT and TD-DFT calculations. Thus, while the investigation of the one-electron oxidized species delivers the noninnocent character of the corrole ring, the knowledge of the electron structure of the one-electron reduced species delivers information about the noninnocent nature of NO, the oldest known noninnocent ligand. Our results here reveal that spectroelectrochemistry is a very useful technique for investigating metal complexes containing several potentially noninnocent ligands. This combined approach can be used to establish the electronic structures of such metal complexes in their various redox states. Information obtained from such

dx.doi.org/10.1021/ic402304e | Inorg. Chem. 2014, 53, 1417−1429

Table 9. TD-DFT (B3LYP/6-31G*/SDD/CPCM/CH_2Cl_2) Calculated Electronic Transitions for $2B^n$ (n = 1+, 0, 1−)

E/eV	λ/nm (expt) (ε/M^{-1} cm^{-1})	λ/nm (DFT) (f)	transitions	character
		2B (S = 0)		
5.5055	225(40100)	225(0.1098)	HOMO-7 → LUMO+5 (0.48)	cor(π) → cor(π^*)
4.7106	262(24700)	263(0.0422)	HOMO-2 → LUMO+6 (0.49)	cor(π) → cor(π^*)
3.0014	390(56200)	413(0.4615)	HOMO-5 → LUMO (0.50)	cor(π) → Fe(dπ)
2.4125	533(8500)	514(0.0012)	HOMO-14 → LUMO (0.38)	cor(π) → Fe(dπ)
		2B$^+$ (S = 1/2)		
2.8725	399(38000)	432(0.0084)	HOMO-3(α) → LUMO+2(α)(0.46)	cor(π) → cor(π^*)
1.9501	637(3700)	636(0.0121)	HOMO-12(α) → LUMO(α) (0.27)	cor(π) → cor(π^*)
			HOMO(β) → LUMO+1(β) (0.18)	cor(π) → cor(π^*)
		2B$^-$ (S = 1/2)		
3.8637	330(24100)	321(0.0539)	HOMO-8(α) → LUMO+1(α) (0.45)	Fe(dπ) → cor(π^*)
2.8912	422(40700)	429(0.0229)	HOMO-2(β) → LUMO+13(β) (0.48)	NO(π)/cor(π) → cor(π^*)
2.1770	570(12000)	569(0.0168)	HOMO-1(β) → LUMO(β) (0.44)	cor(π) → cor(π^*)
			HOMO-1(β) → LUMO+1(β)(0.42)	cor(π) → cor(π^*)
1.9751	633(7000)	628(0.0646)	HOMO(β) → LUMO+3(β) (0.51)	cor(π) → cor(π^*)
1.5899	765(2100)	780(0.0022)	HOMO-1(β) → LUMO(β) (0.62)	cor(π) → cor(π^*)
			HOMO-1(α) → LUMO(α) (0.60)	cor(π) → cor(π^*)

studies is often useful while investigating the relevance of such complexes in redox catalysis. Future work from our laboratories will be focused on those directions.

■ ASSOCIATED CONTENT

Supporting Information

ESI−MS spectra of **2A**, **3A**, and **2B**. ^{1}H NMR spectrum of **3A**, and **1B**. ^{13}C NMR spectra of **1B**, **2B**, **3B**, and **3A**. Packing diagrams of **1B** and **2B**. Electronic absorption spectra of **1B**, **2B**, and **3B**. UV−vis, IR, and EPR spectroelectrochemical measurements of **1B** and **2B**. Electronic absorption and emission spectra of **3A**. This material is available free of charge via the Internet at http://pubs.acs.org.

■ AUTHOR INFORMATION

Corresponding Authors

*(G.K.L.) E-mail: lahiri@chem.iitb.ac.in.
*(B.S.) E-mail: Biprajit.Sarkar@fu-berlin.de.
*(S.K.) E-mail: sanjib@niser.ac.in.

Notes

The authors declare no competing financial interest.

■ ACKNOWLEDGMENTS

Financial support received from the Department of Atomic Energy (India) is gratefully acknowledged. S.K. thanks DST-New Delhi for partial funding. Authors thankfully acknowledge NISER, Bhubaneswar and IOP, Bhubaneswar for providing infrastructure and instrumental support. Fonds der chemischen Industrie (FCI) is kindly acknowledged for financial support.

■ REFERENCES

(1) (a) Arnold, W. P.; Mittal, C. K.; Katsuki, S.; Murad, F. *Proc. Natl. Acad. Sci. U.S.A.* **1977**, *74*, 3203. (b) Wolin, M. S.; Wood, K. S.; Ignarro, L. J. *J. Biol. Chem.* **1982**, *257*, 3312.

(2) Sundaresan, M.; Yu, Z. X.; Ferrans, V. J.; Irani, K.; Finkel, T. *Science* **1995**, *270*, 296.

(3) (a) *Basic EPR Methodology in Nitric Oxide Research from Chemistry to Biology*; Henry, Y., Guissani, A., and Ducastel, B., Eds.; Springer, Austin, TX, 1997; pp 61−86, (b) Olson, L. W.; Schaeper, D.; Lanpn, D.; Kadish, K. M. *J. Am. Chem. Soc.* **1982**, *104*, 2042. (c) Lanpn, D.; Kadish, K. M. *J. Am. Chem. Soc.* **1983**, *105*, 5610. (d) Mu, X. H.; Kadish, K. M. *Inorg. Chem.* **1988**, *27*, 4720. (e) Choi, L. K.; Liu, Y.; Feng, D.; Paeng, K.-J.; Ryan, M. D. *Inorg. Chem.* **1991**, *30*, 1832.

(4) Ozawa, S.; Fujii, H.; Morishima, I. *J. Am. Chem. Soc.* **1992**, *114*, 1548.

(5) (a) *The Porphyrin Handbook*; Kadish, K. M., Smith, K. M., Guilard, R., Eds.; Academic Press: New York, 1959−2003; Vol. *1*−*20*. (b) Steene, E.; Wondimagegn, T.; Ghosh, A. *J. Phys. Chem. B* **2001**, *105*, 11406. (c) Cai, S.; Licoccia, S.; Walker, F. A. *Inorg. Chem.* **2001**, *40*, 5795. (d) Ramdhanie, B.; Zakharov, L. N.; Rheingold, A. R.; Goldberg, D. P. *Inorg. Chem.* **2002**, *41*, 4105. (e) Kadish, K. M.; Fremond, L.; Ou, Z.; Shao, J.; Shi, C.; Anson, F. C.; Burdet, F.; Gros, C. P.; Barbe, J.-M.; Guilard, R. *J. Am. Chem. Soc.* **2005**, *127*, 5625. (f) Edwards, N. Y.; Eikey, R. A.; Loring, M. I.; Abu-Omar, M. M. *Inorg. Chem.* **2005**, *44*, 3700. (g) Collman, J. P.; Decreau, R. A. *Org. Lett.* **2005**, *7*, 975. (h) Gryko, D. T.; Fox, J. P.; Goldberg, D. P. *J. Porphyrins Phthalocyanines* **2004**, *8*, 1091. (i) Sessler, J. L.; Weghorn, S. J. In *Expanded, Contracted & Isomeric Porphyrins*; Baldwin, J. E., Ed.; Tetrahedron Organic Chemistry Series, Pergamon: New York, 1997; Vol. *18*; pp 11−120. (j) Vogel, E.; Will, S.; Tilling, A. S.; Neumann, L.; Lex, J.; Bill, E.; Trautwein, A. X.; Wieghardt, K. *Angew. Chem., Int. Ed. Engl.* **1994**, *33*, 731. (k) Caemelbecke, E. V.; Will, S.; Autret, M.; Adamian, V. A.; Lex, J.; Gisselbrecht, J.-P.; Gross, M.; Vogel, E.; Kadish, K. M. *Inorg. Chem.* **1996**, *35*, 184. (l) Gross, Z.; Galili, N.; Simkhovich, L.; Saltsman, I.; Botoshansky, M.; Blaser, D.; Boese, R.; Goldberg, I. *Org. Lett.* **1999**, *1*, 599. (m) Meier-Callahan, A. E.; Di Bilio, A. J.; Simkhovich, L.; Mohammed, A.; Goldberg, I.; Gray, H. B.; Gross, Z. *Inorg. Chem.* **2001**, *40*, 6788. (n) Mohammed, A.; Gray, H. B.; Meier-Callahan, A. E.; Gross, Z. *J. Am. Chem. Soc.* **2003**, *125*, 1162. (o) Hoshino, M.; Ozawa, K.; Seki, H.; Ford, P. C. *J. Am. Chem. Soc.* **1993**, *115*, 9568. (p) Hoshino, M.; Maeda, M.; Konishi, R.; Seki, H.; Ford, P. C. *J. Am. Chem. Soc.* **1996**, *118*, 5702. (q) Laverman, L. E.; Hoshino, M.; Ford, P. C. *J. Am. Chem. Soc.* **1997**, *119*, 12663. (r) Lorkovic, I. M.; Ford, P. C. *Inorg. Chem.* **1999**, *38*, 1467. (s) Lorkovic, I. M.; Ford, P. C. *J. Am. Chem. Soc.* **2000**, *122*, 6516. (t) Laverman, L. E.; Wanat, A.; Oszajca, J.; Stochel, G.; Ford, P. C.; van Eldik, R. *J. Am. Chem. Soc.* **2001**, *123*, 285. (u) Laverman, L. E.; Ford, P. C. *J. Am. Chem. Soc.* **2001**, *123*, 11614. (v) Kurtikyan, T. S.; Martirosyan, G. G.; Lorkovic, I. M.; Ford, P. C. *J. Am. Chem. Soc.* **2002**, *124*, 10124. (w) Fernandez, B. O.; Ford, P. C. *J. Am. Chem. Soc.* **2003**, *125*, 10510. (x) Patterson, J C.; Lorkovic, I. M.; Ford, P. C. *Inorg. Chem.* **2003**, *42*, 4902. (y) Fernandez, B. O.; Lorkovic, I. M.; Ford, P. C. *Inorg. Chem.* **2004**, *43*, 5393. (z) Nardis, S.; Stefanelli, M.; Mohite, P.; Pomarico, G.; Tortora, L.; Manowong, M.; Chen, P.; Kadish, K. M.; Fronczek, F. R.; McCandless, G. T.; Smith, K. M.; Paolesse, R. *Inorg. Chem.* **2012**, *51*, 3910. (z1) Pomarico, G.; Fronczek, F. R.; Nardis, S.; Smith, K. M.; Paolesse, R. *J. Porphyrins Phthalocyanines* **2011**, *15*, 1085.

(z2) Stefanelli, M.; Nardis, S.; Tortora, L.; Fronczek, F. R.; Smith, K. M.; Licoccia, S.; Paolesse, R. *Chem. Commun.* **2011**, *47*, 4255. (z3) Harischandra, D. N.; Zhang, R.; Newcomb, M. *J. Am. Chem. Soc.* **2005**, *127*, 13776. (z4) Simkhovich, L.; Mahammed, A.; Goldberg, I.; Gross, Z. *Chem.—Eur. J.* **2001**, *7*, 1041. (z5) Simkhovich, L.; Gross, Z. *Tetrahedron Lett.* **2001**, *42*, 8089. (z6) Steene, E.; Wondimagegn, T.; Ghosh, A. *J. Phys. Chem. B* **2001**, *105*, 11406.

(6) (a) Zyska, B.; Schwalbe, M. *Chem. Commun.* **2013**, *49*, 3799. (b) Graham, D. J.; Dogutan, D. K.; Schwalbe, M.; Nocera, D. G. *Chem. Commun.* **2012**, *48*, 4175. (c) Schwalbe, M.; Dogutan, D. K.; Stoian, S. A.; Teets, T. S.; Nocera, D. G. *Inorg. Chem.* **2011**, *50*, 1368. (d) Biswas, A. N.; Das, P.; Agarwala, A.; Bandyopadhyay, D.; Bandyopadhyay, P. *J. Mol. Catal. A: Chem.* **2010**, *326*, 94. (e) Pan, Z.; Harischandra, D. N.; Newcomb, M. *J. Inorg. Biochem.* **2009**, *103*, 174. (f) Ye, S.; Tuttle, T.; Bill, E.; Simkhovich, L.; Gross, Z.; Thiel, W.; Neese, F. *Chem.—Eur. J.* **2008**, *14*, 10839. (g) Collman, J. P.; Kaplun, M.; Decreau, R. A. *Dalton Trans.* **2006**, *4*, 554. (h) Harischandra, D. N.; Zhang, R.; Newcomb, M. *J. Am. Chem. Soc.* **2005**, *127*, 13776. (i) Nardis, S.; Paolesse, R.; Licoccia, S.; Fronczek, F. R.; Vicente, M. G. H.; Shokhireva, T. K.; Cai, S.; Walker, F. A. *Inorg. Chem.* **2005**, *44*, 7030. (j) Simkhovich, L.; Gross, Z. *Inorg. Chem.* **2004**, *43*, 6136. (k) Steene, E.; Dey, A.; Ghosh, A. *J. Am. Chem. Soc.* **2003**, *125*, 16300. (l) Cai, S.; Licoccia, S.; D'Ottavi, C.; Paolesse, R.; Nardis, S.; Bulach, V.; Zimmer, B.; Shokhireva, T. Kh.; Ann Walker, F. *Inorg. Chim. Acta* **2002**, *339*, 171. (m) Zakharieva, O.; Schuenemann, V.; Gerdan, M.; Licoccia, S.; Cai, S.; Walker, F. A.; Trautwein, A. X. *J. Am. Chem. Soc.* **2002**, *124*, 6636. (n) Steene, E.; Wondimagegn, T.; Ghosh, A. *J. Phys. Chem. B* **2001**, *105*, 11406. (o) Simkhovich, L.; Galili, N.; Saltsman, I.; Goldberg, I.; Gross, Z. *Inorg. Chem.* **2000**, *39*, 2704. (p) Mahammed, A.; Gray, H. B.; Weaver, J. J; Sorasaenee, K.; Gross, Z. *Bioconjugate Chem.* **2004**, *15*, 738. (q) Mahammed, A.; Gross, Z. *J. Am. Chem. Soc.* **2005**, *127*, 2883.

(7) (a) Autret, M.; Will, S.; Caemelbecke, E. V.; Lex, J.; Gisselbrecht, J.-P.; Gross, M.; Vogel, E.; Kadish, K. M. *J. Am. Chem. Soc.* **1994**, *116*, 9141. (b) Singha, P.; Saltsmana, I.; Mahammeda, A.; Goldberg, I.; Tumanskiia, B.; Gross, Z. *J. Porphyrins Phthalocyanines* **2012**, *16*, 663. (c) Joseph, C.; Ford, P. C. *J. Am. Chem. Soc.* **2005**, *127*, 6737. (d) Joseph, C. A.; Lee, M. S.; Iretskii, A. V.; Wu, G.; Ford, P. C. *Inorg. Chem.* **2006**, *45*, 2075. (e) Broering, M.; Milsmann, C.; Ruck, S.; Koehler, S. *J. Organomet. Chem.* **2009**, *694*, 1011. (f) Simkhovich, L.; Goldberg, I.; Gross, Z. *Inorg. Chem.* **2002**, *41*, 5433.

(8) Enemark, J. H.; Feltham, R. D. *Coord. Chem. Rev.* **1974**, *13*, 339.

(9) Koszarna, B.; Gryko, D. T. *J. Org. Chem.* **2006**, *71*, 3707.

(10) Paolesse, R.; Nardis, S.; Sagone, F.; Khoury, R. G. *J. Org. Chem.* **2001**, *66*, 550.

(11) Krejcik, M.; Danek, M.; Hartl, F. *J. Electroanal. Chem.* **1991**, *317*, 179.

(12) Sheldrick, G. M. *Acta Crystallogr.* **2008**, *A64*, 112.

(13) van der Sluis, P.; Spek, A. L. *Acta Crystallogr., Sect. A* **1990**, *46*, 194.

(14) Lee, C.; Yang, W.; Parr, R. G. *Phys. Rev. B: Condens. Matter* **1988**, *37*, 785–789.

(15) (a) Andrae, D.; Haeussermann, U.; Dolg, M.; Stoll, H.; Preuss, H. *Theor. Chim. Acta* **1990**, *77*, 123–141. (b) Fuentealba, P.; Preuss, H.; Stoll, H.; Von, S. L. *Chem. Phys. Lett.* **1982**, *89*, 418–422.

(16) Frisch, M. J.; Trucks, G. W.; Schlegel, H. B.; Scuseria, G. E.; Robb, M. A.; Cheeseman, J. R.; Scalmani, G.; Barone, V.; Mennucci, B.; Petersson, G. A.; Nakatsuji, H.; Caricato, M.; Li, X.; Hratchian, H. P.; Izmaylov, A. F.; Bloino, J.; Zheng, G.; Sonnenberg, J. L.; Hada, M.; Ehara, M.; Toyota, K.; Fukuda, R.; Hasegawa, J.; Ishida, M.; Nakajima, T.; Honda, Y.; Kitao, O.; Nakai, H.; Vreven, T.; Montgomery, J. A., Jr.; Peralta, J. E.; Ogliaro, F.; Bearpark, M.; Heyd, J. J.; Brothers, E.; Kudin, K. N.; Staroverov, V. N.; Kobayashi, R.; Normand, J.; Raghavachari, K.; Rendell, A.; Burant, J. C.; Iyengar, S. S.; Tomasi, J.; Cossi, M.; Rega, N.; Millam, N. J.; Klene, M.; Knox, J. E.; Cross, J. B.; Bakken, V.; Adamo, C.; Jaramillo, J.; Gomperts, R.; Stratmann, R. E.; Yazyev, O.; Austin, A. J.; Cammi, R.; Pomelli, C.; Ochterski, J. W.; Martin, R. L.; Morokuma, K.; Zakrzewski, V. G.; Voth, G. A.; Salvador, P.; Dannenberg, J. J.; Dapprich, S.; Daniels, A. D.; Farkas, Ö.; Foresman, J. B.; Ortiz, J. V.; Cioslowski, J.; Fox, D. J. *Gaussian09*, revision A.02; Gaussian, Inc.: Wallingford, CT, 2009.

(17) (a) Bauernschmitt, R.; Ahlrichs, R. *Chem. Phys. Lett.* **1996**, *256*, 454–464. (b) Stratmann, R. E.; Scuseria, G. E.; Frisch, M. J. *J. Chem. Phys.* **1998**, *109*, 8218–8224. (c) Casida, M. E.; Jamorski, C.; Casida, K. C.; Salahub, D. R. *J. Chem. Phys.* **1998**, *108*, 4439–4449.

(18) (a) Barone, V.; Cossi, M. *J. Phys. Chem. A* **1998**, *102*, 1995–2001. (b) Cossi, M.; Barone, V. *J. Chem. Phys.* **2001**, *115*, 4708–4717. (c) Cossi, M.; Rega, N.; Scalmani, G.; Barone, V. *J. Comput. Chem.* **2003**, *24*, 669–681.

(19) Leonid, S. *Chemissian 1.7*; 2005–2010; http://www.chemissian.com.

(20) Zhurko, D. A.; Zhurko, G. A. *ChemCraft 1.5*; Plimus: San Diego, CA, http://www.chemcraftprog.com.

(21) Lee, C.-H.; Lindsey, J. S. *Tetrahedron* **1994**, *50*, 11427.

(22) Balazs, Y. S.; Saltsman, I.; Mahammed, A.; Tkachenko, E.; Golubkov, G.; Levine, J.; Gross, Z. *Magn. Reson. Chem.* **2004**, *42*, 624.

(23) (a) Dastidar, P.; Goldberg, I. *Acta Crystallogr.* **1996**, *C52*, 1976. (b) Musah, R. A.; Jensen, G. M.; Rosenfeld, R. J.; McRee, D. E.; Goodin, D. B. *J. Am. Chem. Soc.* **1997**, *119*, 9083. (c) Desiraju, G. R. *Acc. Chem. Res.* **1996**, *29*, 441. (d) Byrn, M. P.; Curtis, C. J.; Khan, S. I.; Sawin, P. A.; Tsurumi, R.; Strouse, C. E. *J. Am. Chem. Soc.* **1990**, *112*, 1865. (e) Sugiura, K.; Ushiroda, K.; Tanaka, T.; Sawada, M.; Sakata, Y. *Chem. Lett.* **1997**, 927. (f) Mingos, D. M. P.; Sherman, D. J. *Adv. Inorg. Chem.* **1989**, *34*, 293.

(24) Singh, P.; Das, A. K.; Sarkar, B.; Niemeyer, M.; Roncaroli, F.; Olabe, J. A.; Fiedler, J.; Zális, S.; Kaim, W. *Inorg. Chem.* **2008**, *47*, 7106–7113.